HHS Public Access

An optimized fluorescent probe for visualizing glutamate neurotransmission

Jonathan S. Marvin[1], **Bart G. Borghuis**[1,2], **Lin Tian**[1,7], **Joseph Cichon**[3], **Mark T. Harnett**[1], **Jasper Akerboom**[1], **Andrew Gordus**[4], **Sabine L. Renninger**[5], **Tsai-Wen Chen**[1], **Cornelia I. Bargmann**[4], **Michael B. Orger**[5], **Eric R. Schreiter**[1], **Jonathan B. Demb**[2,6], **Wen-Biao Gan**[3], **S. Andrew Hires**[1], and **Loren L. Looger**[1,†]

[1] Howard Hughes Medical Institute, Janelia Farm Research Campus, Ashburn, VA 20147, USA

[2]Department of Ophthalmology and Visual Science, Yale University School of Medicine, New Haven, CT 06511, USA

[3]Skirball Institute of Biomolecular Medicine, New York University School of Medicine, New York, NY 10016, USA

[4]Howard Hughes Medical Institute, The Rockefeller University, New York, NY 10065, USA

[5]Champalimaud Neuroscience Programme, Champalimaud Centre for the Unknown, Av. Brasília, Doca de Pedrouços, 1400-038 Lisboa, Portugal

[6]Department of Cellular & Molecular Physiology, Yale University School of Medicine, New Haven, CT 06511, USA

Abstract

We describe an intensity-based glutamate-sensing fluorescent reporter ("iGluSnFR") with signal-to-noise ratio and kinetics appropriate for *in vivo* imaging. We engineered iGluSnFR *in vitro* to maximize its fluorescence change, and validated its utility for visualizing glutamate release by neurons and astrocytes in increasingly intact neurological systems. In hippocampal culture,

†Correspondence should be addressed to L. L. L. (loogerl@janelia.hhmi.org).
[7]current address: Department of Biochemistry and Molecular Medicine, University of California Davis School of Medicine, Sacramento CA 95817, USA

Construct availability

Competing interests

iGluSnFR detected single field stimulus-evoked glutamate release events. In pyramidal neurons in acute brain slices, glutamate uncaging at single spines showed that iGluSnFR responds robustly and specifically to glutamate *in situ*, and responses correlate with voltage changes. In mouse retina, iGluSnFR-expressing neurons showed intact light-evoked excitatory currents, and the sensor revealed tonic glutamate signaling in response to light stimuli. In worms, glutamate signals preceded and predicted post-synaptic calcium transients. In zebrafish, iGluSnFR revealed spatial organization of direction-selective synaptic activity in the optic tectum. Finally, in mouse forelimb motor cortex, iGluSnFR expression in layer V pyramidal neurons revealed task-dependent single-spine activity during running.

Keywords

Glutamate; functional imaging; neurotransmitter release; biosensor; genetically encoded neural activity indicator

Introduction

Glutamate is among the most important signaling molecules in all kingdoms of life. Glutamate-gated ion channels exist in a number of non-animal species ranging from bacteria to plants. In the nervous system of animals, such channels (ionotropic glutamate receptors, iGluRs) form the cornerstone of information transmission at glutamatergic synapses. Extra-synaptic glutamate signaling ("spillover") activates both ionotropic and metabotropic glutamate receptors (mGluRs), located pre- and peri-synaptically, and also along the axonal sheath[1]. In addition to its normal role in trans- and extra-synaptic transmission, glutamate is both received and released by astrocytes[2], the primary type of glial cell in the brain. Neuronal glutamate release mediates glial Ca^{2+} currents, directing their secretion of glutamate, ATP, and D-serine, which provide feedback to regulate local neurons and vascular cells[3]. Dysregulation of glutamate is implicated in receptor-mediated excitotoxicity, most notably following stroke and traumatic brain/spinal cord injury[4], and in the progression of chronic neurodegenerative disorders such as glaucoma, Alzheimer's, Huntington's, and Parkinson's diseases[5].

Existing tools for quantitative measurement of rapid glutamate transients in intact preparations exhibit poor signal-to-noise ratio (SNR), kinetics, and targetability. Historically, glutamate has been determined primarily by *in situ* microdialysis[6], but this technique is invasive and provides only single-point sampling of bulk tissue with seconds-level temporal resolution. Enzymes such as glutamate dehydrogenase or glutamate oxidase can be coupled to secondary readouts such as NADH fluorescence[7] or current through a microelectrode[8], but these methods lack cellular resolution, have response times on the order of a second, and are confounded by other potential sources of signal.

Biosensors composed of glutamate-binding proteins coupled to a fluorescence readout address many of these concerns. Signal may be unambiguously assigned as glutamate-evoked, with much greater spatial and temporal resolution than diffusible secondary readouts. Modern multi-photon fluorescence microscopy[9] allows fast, high-resolution, non-invasive imaging in awake, behaving animals[10].

A recently developed sensor, "EOS", a hybrid sensor made from the AMPA receptor glutamate-binding core and a small molecule dye, produces a ~1-2% fluorescence increase in mouse somatosensory cortical neurons following limb movement[11,12].

Genetically encoded indicators (for review see ref. 13), based on autocatalytic fluorescent proteins such as GFP, may be easily targeted to specific cellular populations and sub-cellular compartments; they may be delivered by relatively non-invasive techniques such as viral infection or transgenesis; and they are compatible with repeated imaging over many months[14]. Genetically encoded calcium indicators (GECIs) are the most developed, although a growing number of sensors for small molecules are available[15].

Bacterial periplasmic binding proteins (PBPs) provide attractive scaffolds from which to make sensors for small molecule metabolites[16]. *Escherichia coli gltI* encodes the periplasmic component of the ABC transporter complex for glutamate and aspartate. The ligand-dependent conformational change in GltI has previously been used to create glutamate sensors, both from small molecule dyes coupled to single introduced cysteines[17], akin to EOS, and from Förster Resonance Energy Transfer (FRET) between cyan and yellow variants of GFP fused to the two protein termini ("FLIP-E"[18]; "SuperGluSnFR"[19]). FRET sensors present several advantages and drawbacks compared to single-wavelength imaging[20]. Ratiometry facilitates concentration determination, but often lacks sensitivity due to low changes in signal; it simplifies motion correction, but consumes greater spectral bandwidth, limiting multiplex imaging. Single-wavelength indicators, typically based on circularly permuted or split fluorescent proteins (FPs), are an appealing alternative to FRET sensors.

We have recently described an approach for generating high-SNR single-wavelength sensors from PBPs by the insertion of circularly permuted fluorescent proteins[21,22]. We pioneered this technique using the *E. coli* maltose-binding protein MalE (MBP)[21], and extended it to the *E. coli* phosphonate-binding protein PhnD[22]. In both cases, high-resolution X-ray crystal structures were available in both the ligand-free, open and the ligand-bound, closed conformations. Plots of C_α torsion angle differences were used to identify ligand-dependent structural changes in sequentially adjacent residues, with the expectation that such conformational changes would be well suited for modulating the fluorescence of an inserted circularly permuted FP. Both cases resulted in high signal-to-noise sensors, for disaccharides (($\Delta F/F)_{max}$~ 6.5)[21] and for organophosphorous compounds (($\Delta F/F)_{max}$ ~ 1.6)[22], respectively.

Here we report a single-wavelength glutamate sensor ("iGluSnFR") constructed from *E. coli* GltI and cpGFP. iGluSnFR is bright and photostable, with 4.5 ($\Delta F/F)_{max}$ *in vitro*, under both 1- and 2-photon illumination. In increasingly intact preparations, we show that iGluSnFR responds specifically to glutamate *in situ*, is extremely sensitive and fast, correlates with simultaneous electrophysiology, can be used in 2-color imaging, and works robustly for long-term imaging in somata, dendrites and spines in retina, worms, zebrafish, and mice.

Results

Sensor engineering and characterization

Designing intensity-based fluorescent sensors[21,22] requires optimization of two parameters: the insertion site of cpGFP into the binding protein and the composition of the residues adjoining the two ("linkers"). In previous work[21,22], we used quantitative structural analysis of local conformational changes that occur upon ligand binding to choose acceptable insertion positions, and high-throughput screening to optimize the linkers. Although no crystal structures of *E. coli* GltI are available in the PDB, a high-resolution structure of the 99% identical GltI from *Shigella flexneri* has been solved in the glutamate-bound state[23], but not in the ligand-free state. We hypothesized that the structural commonalities of our two previous sensors could be generalized to other PBPs, and that based on the global structural homology of *Shigella* GltI (PDB 2VHA) to MBP, we could apply these generalizations to the selection of insertion sites in GltI (Fig. 1a, Supplementary Figs. 1-7).

Placement of the cpGFP insertion point close to the inter-domain hinge region (after residue 253 of GltI, Supplementary Figs. 1 & 7) followed by screening of mutations to both linkers yielded a variant ("GltI253.L1LV/L2NP") with (F/F)$_{max}$ of 4.5 ± 0.1 (s.d., $n = 5$) (Fig. 1b, Supplementary Fig. 8). Titration of purified protein *in vitro* (Fig. 1b) indicates an affinity of 107 ± 9 μM (s.d., $n = 5$) for glutamate, and 145 ± 18 μM ($n = 3$) for aspartate (which has been identified as a co-neurotransmitter with glutamate in some neurons[24]), and a pK$_a$ of 6.5 in the glutamate-bound and 7.0 in the ligand-free state (Supplementary Fig. 9). It has no detectible affinity for a panel of decoy L-amino acids (glutamine, asparagine, cysteine, arginine, histidine, serine, proline, tryptophan, β-alanine, taurine), neurotransmitters (glycine, GABA, acetylcholine, serotonin, D-serine, dopamine and its metabolic precursor L-DOPA), pharmacological glutamate receptor agonists (AMPA, NMDA, kainate) or antagonists (philanthotoxin PhTx-74, D-AP5, NBQX, CNQX, DNQX, CPP), or a glutamate transporter inhibitor (TBOA) (Supplementary Fig. 10), nor does their presence in a glutamate titration significantly affect sensor function (Supplementary Fig. 10). The on-rate of binding was faster than could be detected by our stopped-flow fluorimeter (Supplementary Fig. 11). The protein is bright and photostable under 2-photon excitation (Supplementary Fig. 12), and similar to 1-photon excitation, has a (F/F)$_{max}$ of 4.5 (Supplementary Fig. 13), but with no change in lifetime (Supplementary Fig. 13). As a preliminary test of the sensor on the surface of mammalian cells (HEK293), the *GltI253.L1LV/L2NP* gene was cloned into the pDisplay vector (Invitrogen) for expression under control of a *CMV* promoter. This construct (Supplementary Fig. 14) encodes an N-terminal mouse immunoglobin κ-chain leader sequence, which directs the protein to the secretory pathway; a hemagglutinin A (HA) epitope tag; the GltI253.L1LV/L2NP protein; a myc epitope tag; and at the C-terminus, a platelet derived growth factor receptor transmembrane helix, which anchors the protein to the plasma membrane, displaying it on the extracellular side. The HA tag significantly decreases (F/F)$_{max}$ in glutamate titrations of soluble protein *in vitro* (Supplementary Fig. 15). Thus a new version of the sensor, ("iGluSnFR"), lacking the HA tag, was cloned into the backbone of the pDisplay vector.

The fluorescence of HEK293 cells transfected with *pCMV.iGluSnFR* was measured in our 2-photon microscope, using a perfusion chamber to efficiently wash cultured cells in HBSS/glutamate solutions. The *in situ* affinity of the sensor on HEK293 cells is 4 ± 1 μM (s.d., $n = 4$) (Fig. 1b), a serendipitous 25-fold increase in affinity from the soluble protein that is in the range expected to be physiologically relevant for measuring neurotransmitter release[25]. Although some fluorescent iGluSnFR is seen inside the cell (presumably endoplasmic reticulum-localized), only membrane-displayed sensor responds to glutamate (Fig. 1c).

Characterization in neurons and astrocytes

To determine the suitability of iGluSnFR for detecting synaptic release, hippocampal astrocyte-neuron co-culture was infected with adeno-associated virus (AAV2/1), under either the human *synapsin-1* promoter to drive expression of iGluSnFR in neurons (*AAV.hSynapsin.iGluSnFR*) or the glial fibrillary acidic protein promoter to drive expression in astrocytes (*AAV.GFAP.iGluSnFR*). Two weeks after infection, confocal fluorescence showed that iGluSnFR was evenly distributed on the extracellular surface of neuronal somata and dendrites (Fig. 2a). Expression of iGluSnFR on the extracellular surface remained fairly stable after 4 weeks (Supplementary Fig. 16). Titration with glutamate in a flow cell indicates an *in situ* affinity of the sensor on the surface of neurons of 4.9 ± 1.3 μM (s.d., $n = 3$ ROIs) (Fig. 1b), with ($F/F)_{max} = 1.03 \pm 0.15$. In astrocytes, the fluorescence of iGluSnFR was uniformly distributed on the membrane of somata and processes, but with some punctae apparent (Fig. 2b).

To test the performance of iGluSnFR in resolving action potential (AP)-evoked glutamate transients, a series of electrical field stimuli at 30 Hz was delivered (1 field stimulus evokes 1 AP, data not shown). iGluSnFR is sensitive enough to detect global glutamate release from single field stimuli, in both somata and processes of neurons (Fig. 2c) and on the surface of astrocytes co-cultured with neurons (Fig. 2d). In neurons, increases in iGluSnFR fluorescence were detected in response to single APs (Fig. 2e, field of view ($F/F)_{max} = 0.14 \pm 0.02$; s.d., $n = 3$ trials); on astrocytes, single AP-induced glutamate release from neurons was reliably detected, but with a lower magnitude change in fluorescence (Fig. 2f, ($F/F)_{max} = 0.07 \pm 0.01$). In both cell types, the peak fluorescence plateaus at higher AP stimuli (20-160 APs) (Fig. 2g, Supplementary Fig. 17). iGluSnFR also showed fast kinetics on both cells (Fig. 2e,f); decay time increases with larger AP stimuli (Supplementary Fig. 17). SNR in neurons is significantly larger than that measured with SuperGluSnFR[19] under similar conditions (Fig. 2e).

To confirm that the observed change in fluorescence is the result of glutamate release, and not an artifact, *e.g.* caused by a change in pH at the synapse, *AAV.hSynapsin.iMaltSnFR*[21], which has a similar pH profile to that of iGluSnFR (Supplementary Figs. 9 & 18) was tested as well, and showed no response (Fig. 2g).

Finally, cultured hippocampal neurons were imaged in a perfusion chamber with 2-photon illumination and subjected to "puffs" of glutamate. After extensive washing with HBSS to restore the sensor to a glutamate-free state (neuronal culture growth media contains 5% FBS and ~100 μM glutamate, Supplementary Fig. 19), a patch pipette filled with 37 μM glutamate and 1 nM AlexaFluor 568 (as a red tracer) was brought near the neurons. A small

amount of the mixture was puffed onto the neurons during continuous perfusion of glutamate-free HBSS by briefly applying positive pressure to the patch pipette (< 200 msec). Green fluorescence was observed to increase rapidly and coincidentally with red fluorescence, and decay just slightly slower than diffusion of the red signal (Fig. 2h). Repeated puffs evoked similar fluorescence responses (Fig. 2h).

Two-photon glutamate uncaging and imaging in brain slices

To characterize the sensitivity and kinetics of iGluSnFR in the context of its applicability for studying mammalian synaptic transmission, we employed two-photon glutamate uncaging and imaging in acute rat hippocampal slices[26]. 2-4 weeks after viral delivery of *AAV.hSynapsin.iGluSnFR* into the hippocampus, infected pyramidal neurons in CA1, CA2 and subiculum were patched and filled with AlexaFluor 594. This anatomical dye enabled glutamate uncaging to be targeted at spine heads located on peri-somatic apical oblique and basal dendrites within ~120 μm of the soma. Linescans were recorded at 600-1200 Hz (excited with a second laser at 920 nm), on the spine heads where glutamate was uncaged (Fig. 3). The whole-cell patch electrode recorded cellular electrical responses in current-clamp mode.

Resting membrane potential of iGluSnFR-expressing pyramidal neurons appeared normal (-65.0 ± 0.5 mV, s.e.m., n = 9 neurons). Large, fast iGluSnFR signals were observed at all spines tested (Fig. 3a,b, n = 28 spines from 9 neurons taken from 5 animals), including at uncaging laser intensities that evoked physiologically-sized EPSPs at the soma[27]. Peak amplitude (Fig. 3c) and time-integrated area (Fig. 3d) of iGluSnFR signals correlated roughly linearly with somatic EPSP amplitude. Single-trial results are shown in Supplementary Fig. 20. Responses to single uncaging pulses were extremely rapid (~5 msec). Strikingly, at some spines iGluSnFR responded to very low uncaging laser intensities that produced no EPSP signals above background (Fig. 3b: light blue trace). Control experiments testing the necessity of MNI-glutamate (Fig. 3e), background glutamate detection (Fig. 3f), and glutamate diffusion (Fig. 3g) yielded the expected results. These experiments indicate that iGluSnFR sensitively and rapidly reports glutamate dynamics at relevant cellular structures within the physiological regime for neurotransmission in intact brain tissue.

Mouse retina in vitro *imaging*

Glutamate is the predominant excitatory neurotransmitter in the mammalian retina[28]. In the inner plexiform layer (IPL), ON-type bipolar cells release glutamate onto ON-type ganglion cells following light increments, whereas OFF-type bipolar cells release glutamate onto OFF-type ganglion cells following light decrements. The ON and OFF bipolar cell axon terminals stratify in separate halves of the IPL: ON bipolar terminals stratify in the proximal half, whereas OFF bipolar terminals stratify in the distal half[28]. The known functional anatomy of glutamate release in the retina was used to test iGluSnFR responses to synaptic activity in an intact neural circuit.

iGluSnFR was expressed in ganglion cells[29] of adult mice (> 4 weeks) by viral transduction of *AAV.hSynapsin.iGluSnFR*. Retinas showed robust iGluSnFR expression in the IPL 14

days post-injection (Supplementary Fig. 21). 14-21 days post-injection, we targeted for whole-cell recording an iGluSnFR-expressing ganglion cell of the OFF-delta type (OFF-Sustained[30]) (Fig. 4a). The voltage-clamped cell showed robust excitatory post-synaptic currents (EPSCs) in response to light stimulation (Fig. 4b), confirming that iGluSnFR does not interfere with excitatory synaptic transmission. Fluorescence responses simultaneously recorded from the dendritic arbor in the OFF stratum of the IPL (Fig. 4a) correlated with EPSCs during the dark phase of the stimulus (Fig. 4b), consistent with glutamate release from OFF bipolar cells.

To confirm that light-evoked fluorescence changes signaled glutamate release, we tested the effect of selectively blocking ON bipolar cells. ON bipolar cells express the sign-inverting mGluR6 receptor at their dendrites, whereas OFF bipolar cells instead express iGluRs[28] . An agonist of mGluR6 receptors, L-AP4, selectively hyperpolarizes ON bipolar cells, blocking their synaptic release, but does not block release from OFF bipolar cells[28]. L-AP4 selectively blocked iGluSnFR signals in the ON stratum of the IPL, but not the OFF stratum, confirming that the iGluSnFR signal depends on glutamate release from bipolar cells (Fig. 4c).

In the presence of steady background light, neurites in the OFF stratum of the IPL showed sparse, spontaneous fluorescence events. The glutamate reuptake inhibitor DL-*threo*-β-benzyloxyaspartate (TBOA, 40 μM), which blocks EAAT1 and EAAT2[31], increased both the amplitude and the decay time constant of these spontaneous fluorescence events (Fig. 4d,e). The increased response in TBOA is consistent with a reduced rate of glutamate removal from the synaptic cleft.

We tested whether iGluSnFR could be used to measure receptive fields of bipolar cells at the level of their synaptic outputs. In response to drifting sine-wave gratings of increasing spatial frequency (Fig. 4f), modulation of the iGluSnFR fluorescence peaked at ~6 cycles/mm. This tuning is consistent with surround inhibition at low spatial frequencies. At high frequencies (>10 cycles/mm), bright and dark stimulus regions cover the receptive field simultaneously and response modulation is reduced (Fig. 4f,g). These measurements are consistent with the known receptive field size of bipolar cells[32,33] .

In vivo *glutamate and calcium signaling in* C. elegans

To demonstrate the *in vivo* functionality of iGluSnFR, it was tested in three animal species: *C. elegans*, zebrafish, and mouse. The nematode *C. elegans* has 302 neurons, many of which are glutamatergic. The left and right AVA neurons are command interneurons located in the head lateral ganglia that play an essential role in the reverse locomotion circuit[34]. AVA is post-synaptic to 40 other neurons[35]. In the nerve ring, AVA makes only post-synaptic connections; nerve ring iGluSnFR signal from AVA should thus be exclusively post-synaptic. AVA expresses NMDA- and AMPA-type iGluRs as well as a glutamate-gated chloride channel[36], but appears not to express EAT-4, the primary vesicular glutamate transporter[37]. Its role as an integrator of pre-synaptic signals and its lack of glutamatergic vesicles make it a useful neuron in which to test the ability of iGluSnFR to report post-synaptic glutamate.

We simultaneously monitored glutamate input into AVA, and AVA somatic calcium, using iGluSnFR and the recently developed red genetically encoded calcium indicator RCaMP[38,39], both under control of the *rig-3* promoter. iGluSnFR expression was strongest along the neuronal process in the nerve ring, and RCaMP1e expression was strongest at the soma (Fig. 5a, b). Fluorescence from the neuronal process in the nerve ring was used to detect glutamate input (from iGluSnFR), and fluorescence from the cell body was used to detect calcium output (from RCaMP). We observed that iGluSnFR responses reliably preceded RCaMP responses (Fig. 5c), consistent with existing evidence that glutamate provides strong excitation to AVA, leading to reversal behavior[40-42].

A delay of a few seconds in the cell body RCaMP1e response likely reflects the indirect relationship between depolarization and calcium, as well as the low affinity and slow rise time of RCaMP1e, which produces a strong fluorescence response only above ~1-2 μM $[Ca^{2+}]$[38]. A simple integrator-type computational model shows a direct correlation between the presumed glutamatergic input measured with iGluSnFR, and the resulting calcium signal inferred by somatic RCaMP (Fig. 5c). A single leaky integrator yields a good fit to the experimental data in amplitude and relative timing (Supplementary Figs. 22 & 23). This relationship supports a circuit model in which glutamatergic input correlates both with the timing and the magnitude of subsequent AVA output, and is consistent with existing circuit diagram models of AVA and the surrounding nerve ring.

To demonstrate that the signal detected by iGluSnFR was specifically related to glutamate release, we examined *eat-4(ky5)* mutants, which are defective in the vesicular glutamate transporter that loads glutamate into synaptic vesicles. AVA calcium transients in *eat-4* mutants were not accompanied by increased fluorescence of iGluSnFR (Fig. 5d, Supplementary Fig. 24), suggesting that iGluSnFR specifically detects a glutamate-associated signal, and not general AVA activity. It should be noted that *eat-4* mutants exhibited a reduced number but normal amplitude of RCaMP calcium transients in AVA neurons, consistent with previous results demonstrating that excitatory glutamatergic transmission is one of several inputs that can activate AVA and backward movement[40-42].

In vivo *imaging in fish and mice*

In larval zebrafish, iGluSnFR reliably reported spatial organization of direction-selective synaptic activity in the optic tectum, consistent with but more rapid than GECIs[43] (Supplementary Figs. 25-27).

To evaluate iGluSnFR functionality in the intact rodent brain, we delivered it to layer V of motor cortex *via* infection of *AAV.hSynapsin.iGluSnFR* in juvenile mice (P20-30) (Fig. 6a). Two weeks after infection, two-photon imaging *in vivo* revealed densely packed, yet resolvable individual dendrites, which were clearly visible in the superficial layers (Fig. 6b). In post-fixed brain slices, confocal imaging in layer V revealed sparse labeling of cells, and individual somata displayed a 'halo'-like expression pattern with iGluSnFR clearly peri-membrane (Supplementary Fig. 28). Neuropil was also strongly labeled.

Following iGluSnFR expression, head-fixing posts were implanted and mice were imaged under resting-awake state or running on a free-floating treadmill (Fig. 6c). Since individual

dendrites are clearly resolvable under low-density labeling conditions, we tested whether glutamate transients could be detected in the apical tuft dendrites of layer V neurons of awake, behaving animals by two-photon microscopy in primary motor cortex (M1), in the region specific to forelimb representation (spatial coordinates taken from refs. (mixture of ketamine and xylazine) mice, we frequently observed spontaneous, repetitive 44,45). In anesthetized glutamate transients over hours (Supplementary Fig. 29), consistent with the observation by microdialysis that ketamine increases extracellular glutamate[46]. In resting-awake animals, we observed numerous transient glutamate events with large (F/F)$_{max}$ (~0.2-0.4, Fig. 7c and Supplementary Fig. 30). Additionally, we detected glutamate transients within single dendritic spines over time during head-fixed running (Fig. 6c).

We next imaged iGluSnFR fluorescence in response to motor tasks. Head-fixed animals were subjected to forward/reverse running on a free-floating treadmill. Fast scanning of small cortical ROIs revealed robust and reliable glutamate responses during running (Fig. 6c,d). Peak iGluSnFR responses are restricted to small regions, whose size (~0.25 μm $\times$ 0.25 μm), shape and proximity to the dendritic shaft are indicative of spine heads (Supplementary Fig. 31). Moreover, iGluSnFR revealed dendritic segments containing multiple spines sensing many glutamate events during trials of forward running (Supplementary Fig. 31). Spines reporting glutamate events on these dendritic segments were clustered on the same branch, but their responses were uncoordinated. Consistent with the fast time-scale of neurotransmission, line scanning of a spine head and its associated dendritic shaft during running showed fast kinetics of a glutamate transient (only on the spine head) that lasted ~50-100 msec (Fig. 6d,e).

Glutamate events were either running-associated or running-direction-associated (i.e. reverse-only or forward-only; Fig. 6f). They typically commenced upon running onset and stopped upon running cessation (Fig. 6g). These glutamate events were highly reproducible during several running trials. Furthermore, we found that local application of tetrodotoxin *via* a small craniotomy (Supplementary Fig. 32) effectively blocked running-related glutamate transients along apical tuft dendrites (Fig. 6h). Intra-peritoneal injection of pilocarpine (a non-selective muscarinic receptor agonist) produced seizures in the mice, and doubled the amplitude of observed glutamate events (Supplementary Fig. 33). Thus, iGluSnFR provides a reliable means for investigating glutamate transients in single dendritic spines as well as dendritic branches in awake behaving mice.

Discussion

Glutamate is not only an important chemical messenger in neurobiology; it has many other signaling roles, is central to amino acid metabolism in plants[47], and is a major industrial fermentation product[48]. Tools for detecting glutamate are thus of broad utility. Classical methods for monitoring glutamate, such as microdialysis, are limited by poor spatial and temporal resolution. Recently developed fluorescent sensors, such as FLIP-E[18], SuperGluSnFR[19], and EOS[11,12], have low signal change and have yet to be used beyond initial proof-of-principle experiments. Recent cell-based sensors of neurotransmitters ("CNiFERs")[49,50] access just the bulk medium and are very slow, allowing only volume transmission to be visualized.

Author Manuscript

Author Manuscript

Author Manuscript

Author Manuscript

In addition to advantages over existing glutamate sensors, iGluSnFR may be better suited than calcium indicators for reporting neuronal input and activity in some situations. Detection of $[Ca^{2+}]$ transients in axon terminals is a common proxy for estimating synaptic release. However, the coupling between pre-synaptic $[Ca^{2+}]$ and transmitter release collapses when vesicle pools are depleted following sustained stimulation[51], and is modified in interesting and more subtle ways by activity-dependent synaptic depression and facilitation. iGluSnFR directly and specifically reports excitatory synaptic release. Post-synaptic iGluSnFR expression should allow determination of the timing and localization of excitatory synaptic input from distinct classes of afferent neurons across a dendritic arbor. Indicator variants with altered affinity may be required for investigating the full complement of glutamatergic synapse types[52]. (The ~4 μM affinity of iGluSnFR precludes quantitation of the millimolar glutamate concentrations estimated following heavy release[53].) Co-expression with a second fluorescent protein should aid in reconstructing morphology of iGluSnFR "hot spots". With improved imaging and analysis methods, we anticipate that iGluSnFR will be embraced as a useful complement to calcium imaging to deconvolve neural activity into its composite molecular signaling events.

Supplementary Material

Refer to Web version on PubMed Central for supplementary material.

Acknowledgements

Abbreviations

iGluSnFR	intensity-based glutamate-sensing fluorescent reporter
FP	fluorescent protein
GFP	green fluorescent protein
PBP	periplasmic binding protein
PDB	protein data bank
SNR	signal-to-noise ratio
AP	action potential
MNI-glutamate	4-methoxy-7-nitroindolinyl-caged-L-glutamate

Bibliography

1. Kullmann DM, Asztely F. Trends Neurosci. 1998; 21:8–14. [PubMed: 9464678]
2. Haydon PG. Nat Rev Neurosci. 2001; 2:185–193. [PubMed: 11256079]
3. Nedergaard M, Ransom B, Goldman SA. Trends Neurosci. 2003; 26:523–530. [PubMed: 14522144]

4. Choi DW. J Neurobiol. 1992; 23:1261–1276. [PubMed: 1361523]

5. Parsons CG, Danysz W, Quack G. Drug News Perspect. 1998; 11:523–569. [PubMed: 15616669]

6. Benveniste H, Drejer J, Schousboe A, et al. J Neurochem. 1984; 43:1369–1374. [PubMed: 6149259]

7. Innocenti B, Parpura V, Haydon PG. J Neurosci. 2000; 20:1800–1808. [PubMed: 10684881]

8. Hu Y, Mitchell KM, Albahadily FN, et al. Brain Res. 1994; 659:117–125. [PubMed: 7820652]

9. Denk W, Svoboda K. Neuron. 1997; 18:351–357. [PubMed: 9115730]

10. Kerr JN, Denk W. Nat Rev Neurosci. 2008; 9:195–205. [PubMed: 18270513]

11. Namiki S, Sakamoto H, Iinuma S, et al. Eur J Neurosci. 2007; 25:2249–2259. [PubMed: 17445223]

12. Okubo Y, Sekiya H, Namiki S, et al. Proc Natl Acad Sci USA. 2010; 107:6526–6531. [PubMed: 20308566]

13. Okumoto S. Curr Opin Biotechnol. 2010; 21:45–54. [PubMed: 20167470]

14. Tian L, Hires SA, Mao T, et al. Nat Methods. 2009; 6:875–881. [PubMed: 19898485]

15. Frommer WB, Davidson MW, Campbell RE. Chem Soc Rev. 2009; 38:2833–2841. [PubMed: 19771330]

16. Dwyer MA, Hellinga HW. Curr Opin Struct Biol. 2004; 14:495–504. [PubMed: 15313245]

17. de Lorimier RM, Smith JJ, Dwyer MA, et al. Protein Sci. 2002; 11:2655–2675. [PubMed: 12381848]

18. Okumoto S, Looger LL, Micheva KD, et al. Proc Natl Acad Sci USA. 2005; 102:8740–8745. [PubMed: 15939876]

19. Hires SA, Zhu Y, Tsien RY. Proc Natl Acad Sci USA. 2008; 105:4411–4416. [PubMed: 18332427]

20. Piston DW, Kremers GJ. Trends Biochem Sci. 2007; 32:407–414. [PubMed: 17764955]

21. Marvin JS, Schreiter ER, Echevarria IM, et al. Proteins. 2011; 79:3025–3036. [PubMed: 21989929]

22. Alicea I, Marvin JS, Miklos AE, et al. J Mol Biol. 2011; 414:356–369. [PubMed: 22019591]

23. Hu Y, Fan CP, Fu G, et al. J Mol Biol. 2008; 382:99–111. [PubMed: 18640128]

24. Nadler JV. Neurochem Res. 2011; 36:668–676. [PubMed: 20953700]

25. Clements JD, Lester RA, Tong G, et al. Science. 1992; 258:1498–1501. [PubMed: 1359647]

26. Harnett MT, Makara JK, Spruston N, et al. Nature. 2012; 491:599–602. [PubMed: 23103868]

27. Losonczy A, Magee JC. Neuron. 2006; 50:291–307. [PubMed: 16630839]

28. Miller RF. Invest Ophthalmol Vis Sci. 2008; 49:5184–5198. [PubMed: 19036997]

29. Borghuis BG, Tian L, Xu Y, et al. J Neurosci. 2011; 31:2855–2867. [PubMed: 21414907]

30. Margolis DJ, Detwiler PB. J Neurosci. 2007; 27:5994–6005. [PubMed: 17537971]

31. Shimamoto K, Lebrun B, Yasuda-Kamatani Y, et al. Mol Pharmacol. 1998; 53:195–201. [PubMed: 9463476]

32. Berntson A, Taylor WR. J Physiol. 2000; 524(Pt 3):879–889. [PubMed: 10790165]

33. Schwartz GW, Okawa H, Dunn FA, et al. Nat Neurosci. 2012; 15:1572–1580. [PubMed: 23001060]

34. Chalfie M, Sulston JE, White JG, et al. J Neurosci. 1985; 5:956–964. [PubMed: 3981252]

35. White JG, Southgate E, Thomson JN, et al. Phil Trans R Soc Lond B. 1986; 314:1–340. [PubMed: 22462104]

36. Mellem JE, Brockie PJ, Zheng Y, et al. Neuron. 2002; 36:933–944. [PubMed: 12467596]

37. Brockie PJ, Madsen DM, Zheng Y, et al. J Neurosci. 2001; 21:1510–1522. [PubMed: 11222641]

38. Akerboom J, Carreras N, Tian L, et al. Front Neurosci submitted. 2012

39. Husson SJ, Costa WS, Wabnig S, et al. Curr Biol. 2012; 22:743–752. [PubMed: 22483941]

40. Maricq AV, Peckol E, Driscoll M, et al. Nature. 1995; 378:78–81. [PubMed: 7477293]

41. Brockie PJ, Mellem JE, Hills T, et al. Neuron. 2001; 31:617–630. [PubMed: 11545720]

42. Hart AC, Sims S, Kaplan JM. Nature. 1995; 378:82–85. [PubMed: 7477294]

43. Akerboom J, Chen TW, Wardill TJ, et al. J Neurosci. 2012; 32:13819–13840. [PubMed: 23035093]

44. Yang G, Pan F, Gan WB. Nature. 2009; 462:920–924. [PubMed: 19946265]

45. Tennant KA, Adkins DL, Donlan NA, et al. Cereb Cortex. 2011; 21:865–876. [PubMed: 20739477]

46. Albrecht J, Hilgier W, Zielinska M, et al. Neurochem Res. 2000; 25:1497–1502. [PubMed: 11071369]

47. Forde BG, Lea PJ. J Exp Bot. 2007; 58:2339–2358. [PubMed: 17578865]

48. Sano C. Am J Clin Nutr. 2009; 90:728S–732S. [PubMed: 19640955]

49. Nguyen QT, Schroeder LF, Mank M, et al. Nat Neurosci. 2010; 13:127–132. [PubMed: 20010818]

50. Yamauchi JG, Nemecz A, Nguyen QT, et al. PLoS One. 2011; 6:e16519. [PubMed: 21305050]

51. Singer JH, Diamond JS. J Neurophysiol. 2006; 95:3191–3198. [PubMed: 16452253]

52. Moussawi K, Riegel A, Nair S, et al. Front Sys Neurosci. 2011; 5:94.

53. Clements JD. Trends Neurosci. 1996; 19:163–171. [PubMed: 8723198]
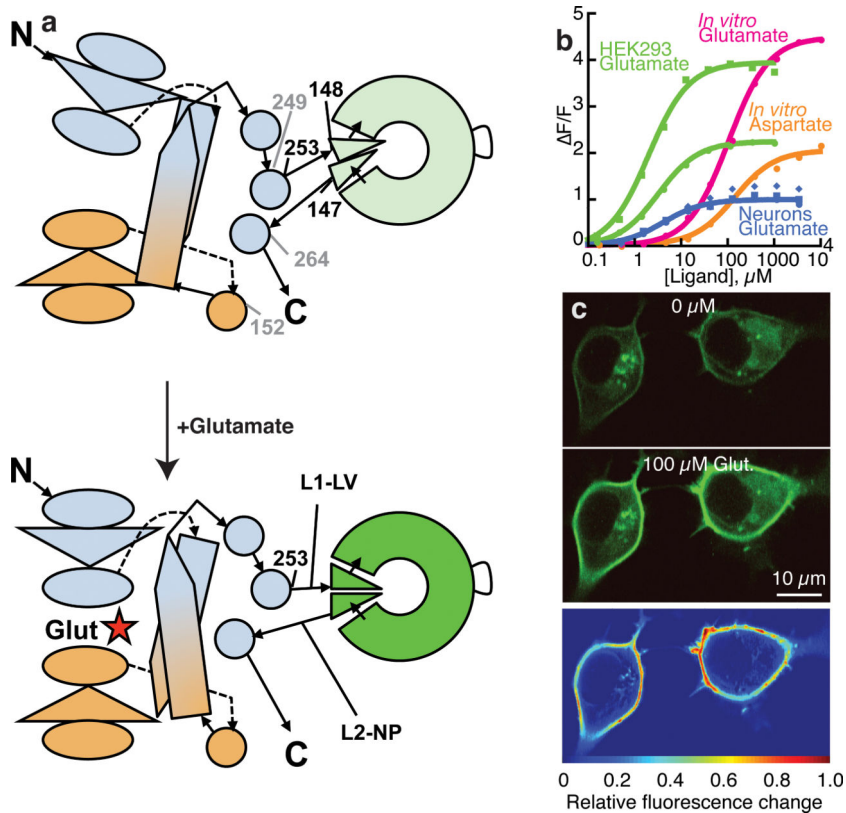
Fig. 1.

Sensor development and in vitro *characterization.* a) Schematic representation of GltI-cpGFP insertion. Residues from both domains (blue and orange) contribute to the binding site for glutamate. The polypeptide chain starts in the N-terminal domain (blue), passes into the C-terminal domain (orange) and back through two beta-strands (long pointed shapes), and into a series of helices (circles). After residue GltI253 (or other residues, identified in gray for "failed" sensors), it enters cpGFP at strand 7 (GFP residue 148), runs through cpGFP, and exits (last GFP residue 147) to rejoin the remainder of GltI. The open (top), ligand-free state of the construct is dim, presumably due to distortion of the cpGFP beta-barrel (tilted triangles). Binding of glutamate (star) induces a conformational change. The closed (bottom) state is bright, presumably due to restoration of the beta-barrel. b) *In vitro* titration of L1LV/L2NP with glutamate (red) and aspartate (orange). *In situ* titration of iGluSnFR on HEK293 cells (green, two ROIs shown) and cultured neurons (blue, three ROIs shown). c) 2-photon fluorescence imaging of HEK293 cells expressing iGluSnFR. The green images are normalized to the peak intensity of the saturated (100 μM glutamate) image. Glutamate strongly increased fluorescence at the cell membrane, but not in intracellular compartments, as shown in the heat map.
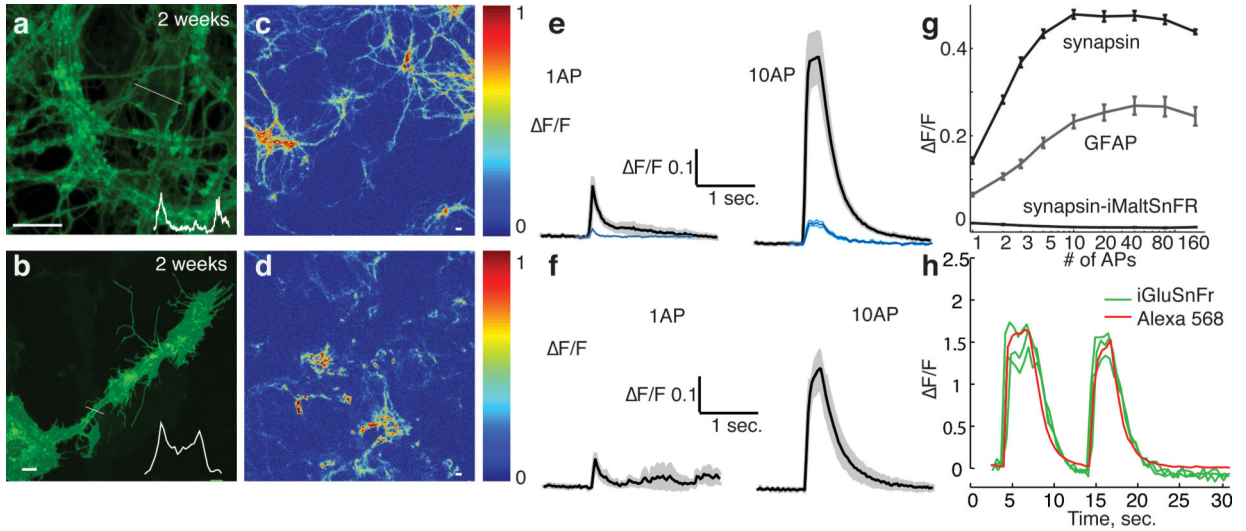
Fig. 2.

Characterization of iGluSnFR in neuron/astrocyte co-culture. iGluSnFR localizes to the
membrane of neurons (a) and astrocytes (b) after expression from *synapsin* and *GFAP*
promoters, respectively, as shown by the intensity profile in white insets. Scale bar, 10 μm.
Field stimulations evoke fluorescent responses in processes and somata of both neurons (c)
and astrocytes (d). Single field stimulus-evoked iGluSnFR responses are easily observable
in both neurons (e; rise $t_{1/2}$ =15 ± 11 msec, decay $t_{1/2}$ =92 ± 11 msec, s.d., *n* = 3 for all
measurements) and astrocytes (f; rise $t_{1/2}$ =30 ± 7 msec, decay $t_{1/2}$ =85 ± 28 msec). Relative
response of SuperGluSnFR reproduced from [19]. The amplitude of response increases with
additional field stimulations, plateauing in cyan at ~10 APs (g); additional stimulations
increase the duration of the fluorescent signal (e,f), but not the amplitude. iMaltSnFR is a
pH-sensitive but glutamate-insensitive control[21]. h) Response of neurons infected with
*AAV.hSynapsin.iGluSnFR* to "puffs" of glutamate/AlexaFluor 568 solution.
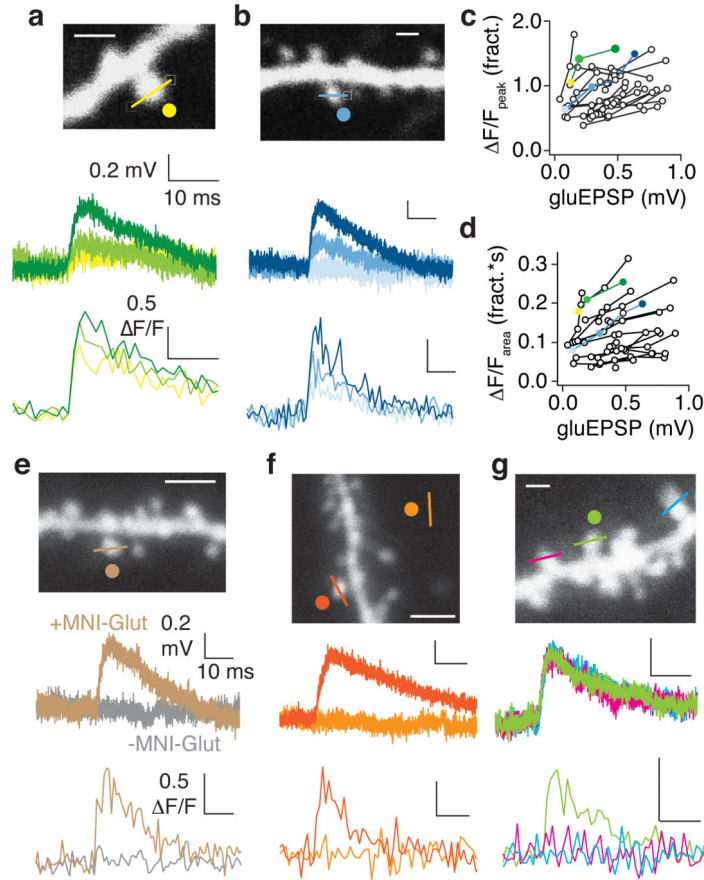
Fig. 3.
Two-photon glutamate uncaging-evoked iGluSnFR signals in acute hippocampal slices.
Two-photon images of apical oblique (a) and basal (b) dendritic branch segments from CA1
hippocampal neurons filled via somatic patch pipettes with AlexaFluor 594. Yellow and
blue symbols indicate locations of linescan through spine heads for iGluSnFR imaging at
920 nm (lines) and focal uncaging of MNI-glutamate at 720 nm (circles). Scale bar: 1 μm.
Trial-averaged (n = 3 to 6) voltage traces recorded at somata (middle trace) and local spine
head iGluSnFR signals (bottom trace) are shown for single pulse (0.2 msec dwell time)
uncaging at three different laser powers. Summary of iGluSnFR signals (c, (F/F)$_{max}$; d,
area) as a function of somatic EPSP amplitude evoked by single pulse two-photon uncaging
for 28 apical oblique and basal dendritic spines, 3 laser powers each. Points connected by
lines represent uncaging at increasing power at individual spines; colors match traces from
(a) and (b). e) iGluSnFR and EPSP signals are substantially decreased when MNI-glutamate
application is discontinued (n = 2). f) Limited iGluSnFR and EPSP signals are observed
when uncaging (circles) and imaging (lines) are performed remotely from the relevant
dendrite (light orange symbols, traces, n = 3). g) Glutamate uncaged at one spine (green)
produces no measurable response in spines > 2 μm away (magenta, blue, n = 4 spines from 2
neurons).

Fig. 4.

Mouse retinal imaging in vitro. a) Two-photon fluorescence images of iGluSnFR-expressing dendrites (green) in the inner plexiform layer (IPL). Top image: z-projection of an iGluSnFR-expressing ganglion cell that was selected for whole-cell recording, and filled with a red fluorescent dye (AlexaFluor 568). Bottom images: single image planes that include the region of interest used for analysis of light-evoked fluorescence responses (dashed white line). b) Simultaneous patch-clamp and fluorescence recording (frame scan, 16 fps) from the cell shown in (a) (average of 8 repetitions, ± s.e.m. for fluorescence shown in grey). Excitatory currents have been inverted for comparison (negative current goes upward). Stimulus was a 150 µm diameter spot, modulated at 100% Michelson contrast (peak wavelength 398 nm). c) L-AP4 (20 µM) blocked glutamate release in the ON- but not in the OFF-layer of the IPL. d) Top, spontaneous fluorescence responses (asterisks) recorded

with line scans (500 lps, ROI contained the cross section of a single, iGluSnFR-expressing dendrite) in the OFF-layer of the IPL during constant background illumination in the absence (top) and presence of TBOA (40 μM, bottom). e) Shape of the average spontaneous fluorescence event in the absence and presence of TBOA ($n = 19$ and 15 events, respectively). f) Fluorescence responses to drifting spatial sine wave stimuli recorded in the ON layer of the IPL (traces show single trials; 90% Michelson contrast). g) Modulation amplitude of the fluorescence response at the drift frequency peaked at a spatial frequency of 6 cycles mm^{-1} (average ± s.e.m. of 6 repetitions).
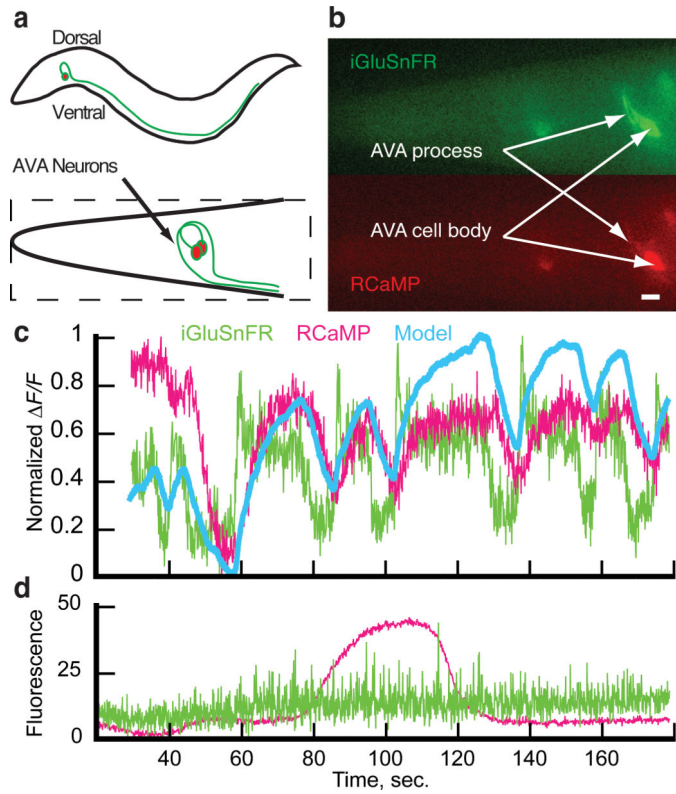
Fig. 5.
Glutamatergic input into *C. elegans* AVA neuron, and resulting somatic [Ca^{2+}] signal. a) Cartoon representation of *C. elegans* and AVA neurons (left and right). Box indicates region imaged in (b). b) Fluorescence micrograph of iGluSnFR and RCaMP1e simultaneously expressed in AVA. Scale bar, 10 μm. c) iGluSnFR fluorescence changes in the process (green) precede somatic RCaMP fluorescence changes (red) during spontaneous AVA activity. The RCaMP response is well fit by a single leaky integrator model (cyan). Fluorescence signals are normalized to baseline and maximum fluorescence in each trace. d) In *eat-4* mutant worms, occasional spontaneous RCaMP activity is seen in AVA, but is unaccompanied by iGluSnFR response.
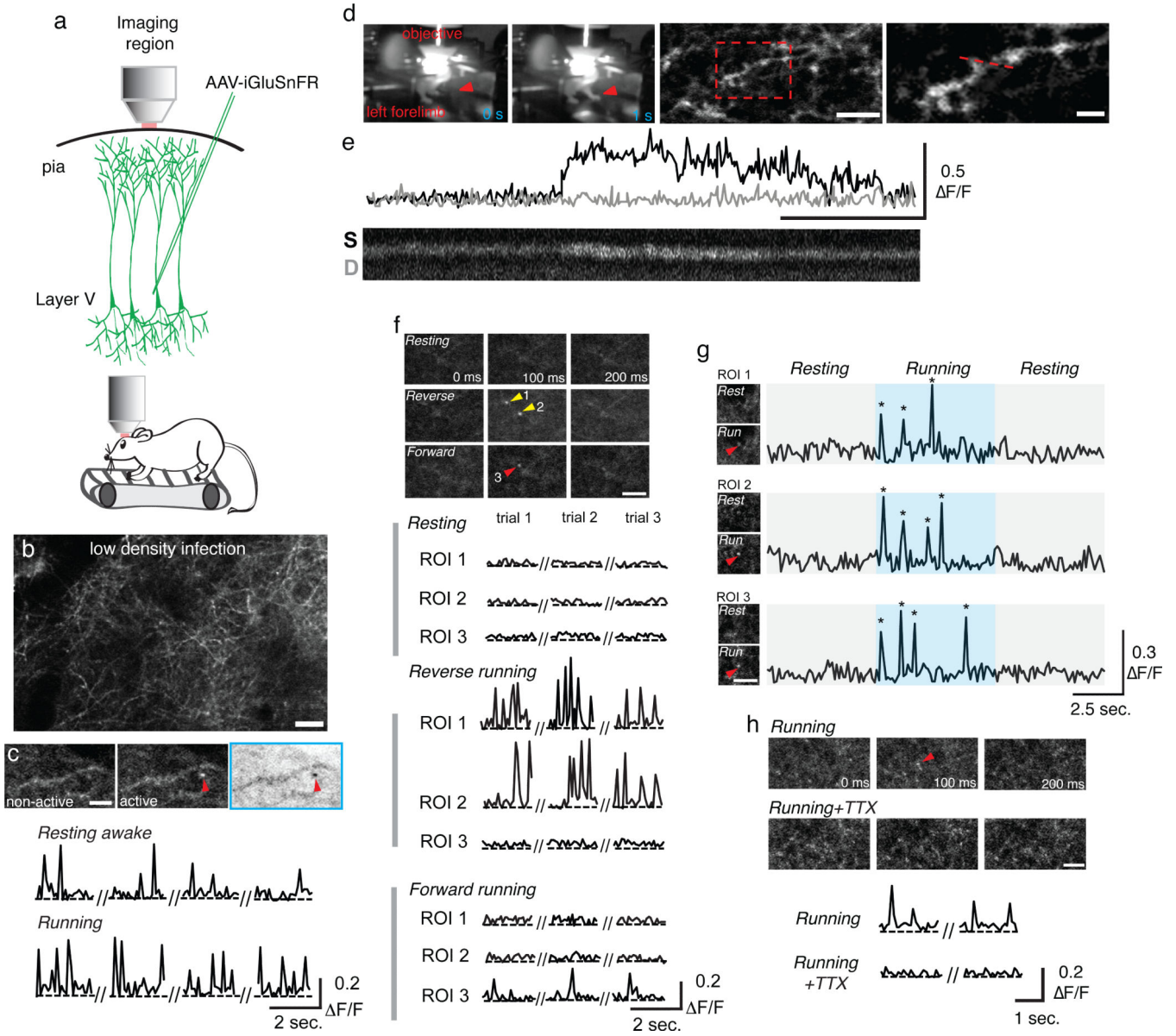
Fig 6.

In vivo imaging of awake behavior and motor task-associated glutamate transients in mouse primary motor cortex. a) Schematic illustrating experimental approach for injection of *AAV.hSynapsin.iGluSnFR* into layer V of primary motor cortex for *in vivo* transcranial two-photon microscopy. b) Two-photon image of low-density infection of primary motor cortex (forelimb region) with *AAV.hSynapsin.iGluSnFR*. Low-density infection results in sparse labeling of apical tuft dendrites of layer V neurons. Scale bar, 10 μm. c) Low-density viral labeling of iGluSnFR revealed apparent dendritic spines (red arrowhead) that show repetitive glutamate transients (four 2 sec. traces shown) during awake resting (top; 7 events over 8 seconds). In this example, forward running increased the frequency of glutamate events (bottom; 15 events detected during running over 8 seconds) and fluorescent changes (average   F/F during running was 27 ± 1.9 s.e.m. vs. 23 ± 3.2 while resting). Scale bar, 2

μm. d) Line scan of a dendritic segment in an awake animal running on the treadmill. Top panels: head-fixed animal undergoing left forelimb movement (red arrowhead) and a two-photon image of a dendritic segment from the apical tuft of motor cortex (scale bar, 5 μm). Boxed region contains the dendritic spine of interest (scale bar, 2 μm). e) Fluorescent trace of line-scan depicted in (d) reveals a rapid and robust glutamate response restricted to a dendritic spine (bottom panel of d); spine, S and black; associated dendrite, D and gray. f) iGluSnFR detection of task-specific glutamate responses during motor training. Example traces of fluorescence changes (2 sec. recordings) during 3 trials of reverse (yellow arrowheads) and forward (red arrowhead) running as well as awake resting state show reverse running triggers repetitive glutamate events with large changes in fluorescence (up to 0.55 (ΔF/F)$_{max}$). No glutamate transients were detected under resting conditions and forward running in ROIs 1 and 2. A different ROI (#3) within the field-of-view activated under forward running conditions. g) iGluSnFR signals correlate with onset and offset of locomotion. *, glutamate events. h) Application of tetrodotoxin (TTX, 1 nM in ACSF) via a small craniotomy lateral to the thinned-skull imaging region (Supplementary Fig. 32) effectively blocked running-related glutamate transients (red arrowhead marks a glutamate transient during running) along apical tuft dendrites. Scale bar, 10 μm.